Presented at the 1st Oaxtepec Symposium
on Nuclear Physics, Mexico City, Mexico,
January 3 - 5, 1978

LBL-7703

CONF-780125--2

FROM NUCLEI TO NUCLEONS

David K. Scott

March 1978

Prepared for the U. S. Department of Energy
under Contract W-7405-ENG-48

MASTER

LAWRENCE BERKELEY LABORATORY
UNIVERSITY OF CALIFORNIA

LBL-7703

DISTRIBUTION OF THIS DOCUMENT IS UNLIMITED

is much longer than the transit time of a nucleon at the Fermi level. The whole nucleus therefore responds coherently to the collision, and the dominant phenomena are characteristic of the mean field. In the high energy regime, the opposite is true. Nucleons undergo such violent collisions with each other that the reactions proceed by independent collisions of the constituent particles. An approximate estimate[3] of the transitional energy can be made as follows. The single particle well U which a nucleon feels when two ions are in close contact is:

$$U = U_A + U_B - \gamma U_A U_B$$

where U_A and U_B are the undisturbed single particle wells (≈50 MeV). The repulsive term arises from the density dependence of the nuclear force. A nucleon with velocity v ($v_F > v > -v_F$, where v_F is the Fermi velocity) is reflected by the edge of the well moving with velocity V, if in the frame attached to the well, its kinetic energy $\frac{1}{2} m(v-V)^2$ is less than E_B. We define v_B by $\frac{1}{2} m v_B^2 = E_B$, and then if $V > V_{cr} = v_B + v_F$ there will be no reflected particles at all. This is the critical velocity above which only two-body collisions are important, and the corresponding energy of the projectile is $E_{cr} \approx 180$ MeV/nucleon. Alternatively we can argue that the upper boundary is set by allowing the two colliding nuclei to overlap completely in momentum space.[2] Since the Fermi sphere has a radius $\approx 1.34\ fm^{-1}$, we find that the projectile must carry an energy ≈ 150 MeV/nucleon. Interesting transitional behavior might therefore be expected to appear at incident energies of several tens of MeV/nucleon. We discuss the first results under three topics: Single particle inclusive measurements of complex fragments; two particle exclusive measurements between light and heavy fragments; single particle inclusive measurements of light fragments.

3. EMISSION OF COMPLEX FRAGMENTS

In organizing the data on the collisions of complex nuclei, experimentalists have relied heavily on the concept of nuclear temperature. For example, at high energies (> 250 MeV/nucleon) a central concept is the nuclear fireball,[4] illustrated schematically in Fig. 1. Nucleons are swept out from the target and projectile to form a quasi-equilibrated system at high temperature, equal to the available energy per nucleon. In the center of mass of the fireball, the emitted particles have the form of a volume[5] Maxwellian distribution:

$$\frac{d^2\sigma}{dEd\Omega} \approx \sqrt{E} \exp(-E/T)$$

The predicted variation[6] of the fireball temperature with energy is shown in Fig. 2 for two assumptions about the mass spectrum of elementary particles created in the fireball. In the bootstrap model, the exponential growth in particles means that particle creation wins over increasing the kinetic energy, and therefore the temperature limits. (This phenomenon has been likened to a phase transition by Hagedorn,[7] who refers to the saturation as the "boiling point" of hadronic matter). For a model based on extrapolating the presently known particle spectrum, the temperature continues to increase. How do these high temperatures connect onto the more familiar nuclear temperatures of one or two MeV?

In low energy nuclear physics, there are two well tested schemes for extracting temperatures; from the energy spectrum as described above, or from the production cross sections of different isotopes. An example[8]

of the latter approach is shown in Fig. 3; here the cross sections for the production of complex fragments in the reaction of $^{16}O + ^{208}Pb$ at E = 137 MeV are plotted versus the two body transfer Q-values Q_{gg}. In a statistical reaction,[9] the cross section is given by:

$$\sigma \approx \rho_f(E^*) \approx \exp\left(\frac{E^*}{T}\right)$$

proportional to the level density of states at excitation $E^* = Q_{gg} - Q$, where the Q value is composed of changes in Coulomb, rotational and other excitation energies. The systematics of Fig. 3 are therefore easily understood[10] if we write:

$$\sigma \approx \exp \frac{Q_{gg} - \Delta V_c}{T}$$

where only the Coulomb term is included in Q (the other terms are not expected to be coupled strongly to the degrees of freedom participating in the equilibrium). The equilibration takes place as the two nuclei rotate in the dinuclear system characteristic of deeply-inelastic scattering. The temperature extracted for the data of Fig. 3 is approximately 2 MeV. We have gathered data at several energies between 1 and 20 MeV/nucleon to study the variation of T with energy. The results[11] are plotted in Fig. 4 with open circles, as a function of MeV/nucleon and also as a function of $\sqrt{E_{cm}-V}$, which is related to the Fermi gas equation of state.

A similar approach can be adopted at energies above 20 MeV/nucleon, except that here the emitter of the complex fragments is more closely allied to the <u>projectile</u>, rather than the rotating dinuclear complex.[12] Then

$$\sigma \approx \sum_i \exp\left(\frac{Q_i}{T}\right)$$

where Q_i are the Q-values for the various fragmentation channels of the projectile. Temperatures extracted in this way for systems similar to $^{16}O + {}^{208}Pb$ at energies of 20 MeV/nucleon,[10] 80 MeV/nucleon[13] 1 GeV/nucleon and 2.1 GeV/nucleon[14] are also shown in Fig. 4 by open circles. We see that the temperature reaches a limiting value of approximately 8 MeV.

The two methods of extracting temperatures in the different energy regimes can be unified by determining the temperature independently by means of the momentum distribution of the fragments.[15,16] In the relativistic region a typical momentum distribution in the projectile rest frame is shown[14] in Fig. 5. In this plot a fragment emerging with the beam velocity would correspond to $P_{11} = 0$ where P_{11} is the longitudinal momentum. The distributions have the form,

$$\frac{d^3\sigma}{dp^3} \approx \exp \frac{-(p-p_0)^2}{2\sigma^2}$$

where $p_0(\approx 0)$ is the momentum at the peak, of width

$$\sigma^2 = \sigma_0^2 \frac{F(A-F)}{(A-1)}$$

F, A are the masses of the observed fragment and the projectile. This value of σ^2 is simply related to the mean square momentum of F nucleons suddenly going off as a single fragment. Not surprisingly, therefore, it is closely related to the Fermi momentum, $p_F = \sigma_0\sqrt{5}$. From the momentum spectrum alone however, it is not possible to distinguish the alternative process of projectile excitation to temperature T, followed by evaporation.[15] (The two extremes can be reconciled in the abrasion-ablation model,[17] which combines a fast process for the production of an excited prefragment with subsequent decay on a slow time scale). For our present purposes it is sufficient to note that the two extreme models are related by:

$$\sigma_0^2 = mT\left(\frac{A-1}{A}\right)$$

where m is the nucleon mass.

We adopt this procedure to evaluate the temperature at <u>all</u> energies from 1 MeV/nucleon to 2 GeV/nucleon, which is tantamount to inferring that the fragments are always observed from projectile decay, although the detailed mechanism of excitation is <u>radically different</u> in the different energy regimes. The above expression for the momentum distribution can be transformed into an energy distribution in the laboratory frame:[18]

$$\frac{d^3\sigma}{dp^3} \rightarrow \frac{d^2\sigma}{dE_L d\Omega} \approx \sqrt{2M_F E_L}\ \exp\left[-\frac{M_F}{\sigma^2}\left(E_L - 2a\, E_L^{\frac{1}{2}} \cos\theta + a^2\right)\right]$$

where $a^2 = \frac{1}{2}M_F\ v_R^2$, the energy corresponding to the peak of the distribution. (This energy is in good agreement with the value expected from fragmentation of the projectile into the observed channels). This function was fitted to our data at each energy ; Fig. 6 shows some representative results for the $^{16}O \rightarrow {}^{12}C + \alpha$ channel. The values of T using the above formulae are plotted in Fig. 4 with closed circles. In all cases the values of T extracted by the two methods are in reasonable agreement, emphasizing the saturation of the temperature at 8 MeV, and the rapid transition towards this limit, which takes place between 10 and 25 MeV/nucleon.

IV. THE LIMITING TEMPERATURE

How are we to interpret this phenomenon? We note that up to incident energies of 10 MeV/nucleon, the temperatures are in reasonable agreement with the Fermi gas equation of state:

$$E^* = aT^2$$

For light nuclei, the level density parameter[19] $a \approx A/8$, with A equal to the mass number of the compound system formed from $^{16}O + {}^{208}Pb$. This agreement is consistent with the model of an equilibrating dinuclear complex, leading to an excited projectile-like prefragment at the same temperature, which then decays. The temperature of 8 MeV must be associated with the heating of a much smaller system since there is insufficient energy for all A nucleons to equilibrate at this temperature. Suppose that the hot emitter in this case consists of A' nucleons. (Our discussion of isotope production cross sections implies that A' must be $\approx$ projectile mass). Further if this system is to succeed in emitting a

complex fragment, it is unlikely that the excitation energy could exceed $8A'$ MeV, on the basis of binding energy considerations. Let us equate,

$$8A' \approx \frac{A'}{8} T^2 .$$

Then we find $T \approx 8$ MeV. In analogy with the discussion of the "boiling point" of hadronic matter in Fig. 2, we can think of 8 MeV as the "boiling point" of nuclear matter. Higher temperatures could lead to an explosion of the system.

An alternative explanation of the limiting temperature is based on the equivalence with the Fermi motion.[15] In a Fermi distribution the average nucleon energy is $\frac{3}{5} p_F^2/2m$, where p_F is the Fermi momentum ($\approx$ 200 MeV/c). Equating this energy to the thermal energy in an equilibrated gas;

$$\frac{3}{2} T = \frac{3}{5} p_F^2/2m$$

we again find $T \approx 8$ MeV. (A similar argument can be applied to complex fragments). The relationship (if any) between the two interpretations of the saturating temperature is an interesting open question at present. Also it appears that higher temperatures may be observed for systems more massive than ^{16}O, and may be related to the distinction between peripherally and centrally dominated collisions.[20] If the initial excitation is localized, similar studies with a heavier projectile could also reveal a lower limiting temperature, as the energy is spread over the more massive system.

V. LOCALIZATION IN HEAVY-ION REACTIONS

Whatever the interpretation of the limiting temperature of 8 MeV, it is clear that the data of Fig. 4 provide evidence for a sudden transition in the nature of the heavy-ion collision in a region approaching the Fermi energy. This energy region is likely to be intimately related to a variety of interesting time constants of nuclear matter. By way of illustration we quote two results from the literature--one very new and one very old. Recent experiments provide evidence for a monopole excitation in nuclei,[21] from which a value of the nuclear compressibility is derived of $K \approx 200$ MeV. The related velocity of sound in nuclear matter[22]

$$v_s = \sqrt{\frac{K}{9m}}$$

where m is the nucleon mass, is roughly 0.15 C, or 11 MeV/nucleon, close to the observed transition region.[23] Also it is interesting to compare the time for emission of a nucleon from a compound system $t_p \approx \exp[c/T]$ with the time for relaxation of energy in nuclear matter. This relaxation time t_R can be written

$$t_R \approx \frac{R^2}{v_F \Lambda}$$

where R is the nuclear dimension, v_F the Fermi velocity and Λ the mean free path. At low temperatures the mean free path is long (for a potential V = 17 MeV, W = 12 MeV, at E = 140 MeV, λ = 5fm), but decreases with increasing temperature according to the relation,

$$\Lambda \sim \frac{1}{\rho\sigma} \left(\frac{E_F}{T}\right)^2$$

(This dependence comes from the fact that the only particles able to alter their states as allowed by the Pauli principle, lie within a spherical velocity shell of radius $\sqrt{2E_F/m}$ and thickness $T/\sqrt{2mE_F}$). These time constants, evaluated in an early calculation,[24] are compared in Fig. 7, which shows that if the system can be brought to temperatures in the region of 7 to 8 MeV, the relaxation time begins to exceed the time for particle emission, and could lead to the formation of a "hot-spot" on the nuclear surface.[25,26] It will be interesting to see whether this concept has any relevance to the transition observed in our data, associated apparently with temperatures approaching 8 MeV. If hot-spots can be observed, specific heats and thermal conductivities of nuclear matter can be deduced,[27] and used to construct alternatives to pre-equilibrium and cascade models. Further insight comes from coincidence experiments.

VI. COINCIDENCE EXPERIMENTS, BETWEEN LIGHT AND HEAVY FRAGMENTS

An experiment on the production of "hot-spots" used the $^{58}Ni + ^{16}O$ reaction at 92 MeV to study the angular correlation between alpha particles and deeply-inelastic scattered products.[28] The correlation is shown in Fig. 8, revealing a pronounced forward angle peaking, in dramatic contrast to the isotropic distribution expected from the equilibrated rotating dinucleus. Considering the rotational motion, there is an angular velocity ω and an angle of rotation θ, through which the fragments remain in contact. Therefore the lifetime is of the order,

$$\tau \approx \theta/\omega \quad .$$

In this case $\theta \approx 2\delta_\theta$, where δ_θ is the width of the distribution, and ω can be estimated from the dynamics of the collision, leading to $\tau \approx 20 \times 10^{-22}$. From Fig. 7, the associated temperature is 3.3 MeV. Using $E^* = aT^2$ with $E^* = 28$ MeV from the experiment, the resultant value of $a \approx N/8$ yields $N \approx 18$ particles. (For the fully equilibrated system $N \approx 70$ and the temperature would only have been 1.8 MeV). We see therefore that emission takes place from a substructure of the dinuclear system, which has tentatively been designated a hot-spot. The mass of this heated region is commensurate with that of the projectile, although in this example the emitted particles were shown to originate from the heavy target-like fragment.

Similar studies have been made of the correlations between light and heavy particles in the ^{16}O + Pb, Au systems at incident energies of approximately 9 and 20 MeV/nucleon.[29] The angular correlations shown in Fig. 9 are also narrow but they are peaked close to direction of the detected projectile-like fragment. A study of the three body kinematics shows that the emission takes place from the projectile-like part of the system. Indeed, the correlation is double-peaked in the case of $^{12}C + \alpha$, indicative of pure projectile fragmentation. However, the correlation patterns for ^{13}C, ^{14}C and ^{14}N which cannot arise from simple projectile fragmentation are very similar in overall shape. They may be associate with emission from a locally heated region, of dimensions commensurate with the projectile, which is formed during the intimate contact of the

two colliding ions. As the incident energy is raised from 8 MeV/nucleon to 20 MeV/nucleon the relative importance of these more complex processes diminishes, and the pure fragmentation channel becomes dominant. The transition takes place in the same region as the rapid temperature change in Fig. 4.

A possible qualitative representation[25] of this behavior is shown in Fig. 10(b), which portrays the "sparking"[30] of nucleons and alpha particles from a locally heated zone in quasi- and deeply-inelastic collisions, by the tangential component of nuclear friction. An alternative mechanism (Fig. 10(a) for the production of fast, non-equilibrium α-particles is the strong radial frictional force which ejects a particle on the opposite side of the nucleus from the initial contact.[31] The contributions of these different mechanisms are not well quantified at present; nor are they the only mechanisms possible for fast nuclear emission, as the last part of this talk will show.

VII. EMISSION OF LIGHT PARTICLES IN HEAVY-ION COLLISIONS

The emission of energetic light particles in heavy-ion collisions is a subject of great interest at the present time, as indeed it has also been in the past.[32] An example of preliminary single proton inclusive spectra from the bombardment of ^{16}O on ^{58}Ni at approximately 10 MeV/nucleon and 20 MeV/nucleon is shown in Fig. 11. At the lower energy the spectra are typical of compound nuclear evaporation.[33] At 20 MeV/nucleon the spectra also have an evaporative shape, extending with substantial cross sections to over 100 MeV energy.

Recently several suggestions have been put forward for possible mechanisms on the production of light particles with velocity much higher than the beam. For example, Fig. 12 shows[34] a heavy-ion reaction with a relative speed V of nucleus 1 at the ion-ion barrier. A nucleon ν moving from nucleus 1 to 2 has, on arrival, a velocity $\underline{v}_2 = \underline{v}_1 + \underline{V}$ where v_1 is its velocity in nucleus 1, with a maximum value equal to $\underline{v}_F + \underline{V}$. The maximum kinetic energy is

$$E(\max) = E_F + E_{rel.} + 2\sqrt{E_F\, E_{rel.}}$$

For a 20 MeV/nucleon collision, with E_F = 35 MeV, E reaches 108 MeV, which is approximately the energy observed in Fig. 11. The characteristics of these preequilibrium particles may give insight in the initial energy loss process in deeply-inelastic collisions. An extension of this model to the study of "Fermi Jets" has recently been developed,[35] and studied experimentally.[36]

The emission of fast light particles is also encountered in time-dependent-Hartree-Fock calculations[37] and in hydrodynamic calculations,[38] examples of which are shown in Fig. 13. A standing wave is set up, and the nucleus fractures at the weakest point, which is the node of a standing wave located at a distance π/k_F from the surface. This phenomenon is related to the tensile strength of nuclear matter.[2]

Another (more trivial) mechanism is excitation and decay of the projectile. For the case illustrated in Fig. 11, an excitation energy up to 35 MeV would be required. There is indeed evidence for this latter type of process in cascade calculations[39] of a similar reaction--192 MeV ^{12}C on ^{56}Fe

(16 MeV/nucleon)--shown as histograms in Fig. 11. An analysis of the cascade revealed that the high energy protons were indeed the result of projectile decay. Cascade calculations are of course often applied to heavy ion collisions at relativistic energies, where the nucleon - nucleon interaction is the dominant collision mechanism, as discussed at the beginning of this talk. Indeed the data used to develop the fireball model (Fig. 1) have also been well described by cascade calculations.[40] (A detailed examination of the cascade process may of course show that the equilibrated fireball description is valid.) The predictions are compared with the data[41] in Fig. 14(a) and (b). It appears therefore that the cascade model can successfully predict the proton spectra at such widely separated energies as 20 MeV/nucleon and 400 MeV/nucleon, and the spectra at both energies have at least a superficial resemblance (see Figs. 11 and 14). The question of when the fireball description ceases to have validity as the incident energy is reduced is a fascinating one within our experimental and theoretical grasp. The answer to the question is intimately related to our earlier discussion of relaxation times, hot-spots and the thermal conductivity of nuclear matter.

VIII. CONCLUSION

Some initial results on heavy-ion collisions in the intermediate energy region between 20 MeV/nucleon and 100 MeV/nucleon were presented and compared to existing data at much lower and much higher energies. At low incident energies the overall potential field determines the evolution of heavy-ion collisions, whereas at high relativistic energies

the nucleon-nucleon processes appear to become dominant. The intermediate region is likely to be fertile territory for understanding the transitional phenomena, although at this early stage the data pose more interesting questions than they answer. Clearly we are seeing the beginning of an area of research which will contribute much to our understanding of characteristic heavy-ion processes as similar experiments with much heavier nuclei become possible in the near future.

IX. ACKNOWLEDGMENTS

Many of the results and interpretations in this paper are of a preliminary nature. The intermediate energy experiments were carried out by the following experimenters: M. Bini, H. Buenerd, S.A. Chessin, P. Doll, C.K. Gelbke, J.V. Geaga, J.Y. Grossiord, D.L. Hendrie, J.L. Laville, J. Mahoney, A. Menchaca-Rocha, M. Mermaz, C. Olmer, L.S. Schroeder, D.K. Scott, T.J.M. Symons, K. Van Bibber, Y.P. Viyogi, and H.H. Wieman.

Work supported by the U. S. Department of Energy.

REFERENCES

1. For a review, see W.U. Schröder and J.R. Huizenga, Ann. Rev. Nucl. Sci. 27, 465 (1977).

2. G. Bertsch, Lecture Notes for the 1977 Les Houches Summer School.

3. H. Orland and R. Schaeffer, J. de Phys. (Lettres)

4. J. Gosset, H.H. Gutrod, W.G. Meyer, A.M. Poskanzer, A. Sandoval, R. Stock, and G.D. Westfall, Phys. Rev. C16, 629 (1977).

5. A. S. Goldhaber, Preprint LBL-7146 (1977).

6. N.K. Glendenning and Y. Karant, Phys. Rev. Lett. 40, 374 (1978).

7. R. Hagedorn, Cargèse Lectures in Physics, Vol. 6, ed. E. Schatzman (Gordon Breach, NY 1973).

8. V.V. Volkov, Sov. J. of Nucl. Phys. 6, 240 (1976).

9. J.P. Bondorf, F. Dickmann, D.H.E. Gross and P.J. Siemens, Symposium on Heavy Ion Reactions and Many Particle Excitations (Saclay, 1971), J. de Phys. 32, C6 (1971).

10. M. Buenerd, C.K. Gelbke, B.G. Harvey, D.L. Hendrie, J. Mahoney, A. Menchaca-Rocha, C. Olmer and D.K. Scott, Phys. Rev. Lett. 37, 1191 (1976).

11. D.K. Scott, M. Bini, P. Doll, C.K. Gelbke, D.L. Hendrie, J.L. Laville, J. Mahoney, A. Menchaca-Rocha, M. Mermaz, C. Olmer, T.J.M. Symons, K. Van Bibber, Y.P.Viyogi and H. Wieman, to be published.

12. V.K. Lukyanov and A.I. Titov, Phys. Lett 57B, 10 (1975).

13. K. Van Bibber, S.A. Chessin, J.V. Geaga, D.L. Hendrie, L.S. Schroeder, D.K. Scott and H.H. Wieman, B.A.P.S. 23, No. 1, 27 (1977) and to be published.

14. D.E. Greiner, P.J. Lindstrom, H.H. Heckman, B. Cork and F.S. Bieser, Phys. Rev. Lett. 35, 152 (1975) and LBL Preprint-3650 (1975).

15. A.S. Goldhaber, Phys. Lett. 53B, 306 (1974).

16. H. Feshbach and K. Huang, Phys. Lett. 47B, 300 (1973).

17. J. Hufner, K. Schafer and B. Schurmann, Phys. Rev. C12, 1888 (1975).

18. C.K. Gelbke, D.K. Scott, M. Bini, D.L. Hendrie, J.L. Laville, J. Mahoney, M.C. Mermaz and C. Olmer, Phys. Lett. 70B, 415 (1977).

19. T.D. Thomas, Ann. Rev. Nucl. Sci. 18, 343 (1968) and refs. therein.

20. G.D. Westfall, R.G. Sextro, A.M. Poskanzer, A.B. Zebelman, G.W. Butler, and E.K. Hyde, LBL-Preprint 6558 (1977).

21. D.H. Youngblood, B.A.P.S. 23, No. 1, 42 (1977).

22. J.A. Maruhn, Proceedings of the Topical Conference on Heavy-Ion Collisions (Falls Creek, Tennessee, 1977). ORNL Report CONF 770602, p. 156.

23. P.J. Siemens, private communication.

24. A. Kind and G. Patergnani, Nuovo Cimento 10, 1375 (1953).

25. H. Bethe, Phys. Rev. 53, 675 (1938).

26. R. Weiner and M. Westrom, Nucl. Phys. A286, 282 (1977).

27. S. Tomonoga, Z. Phys. 110,573 (1938).

28. H. Ho, R. Albrecht, W. Dunnweber, G. Graw, S.G. Steadman, J.P. Wurm, D. Disdier, V. Rauch and F. Schiebling, Z. Phys. A283, 235 (1977).

29. C.K. Gelbke, M. Bini, C. Olmer, D.L. Hendrie, J.L. Laville, J. Mahoney, M.C. Mermaz, D.K. Scott and H.H. Wieman, Phys. Lett. 71B, 83 (1977).

30. J.P. Wurm, Macroscopic Features of Heavy-Ion Collisions and Pre-Equilibrium Processes, (Hakone, Japan 1977), IPCR Report, Supplement 6, 1977, p. 108.

31. D.H.E. Gross and J. Wilczynski, Phys. Lett. 67B, 1 (1977).

32. H.C. Britt and A.R. Quinton, Phys. Rev. 124, 877 (1961).

33. D.V. Reames, Phys. Rev. 137, B332 (1965).

34. J.P. Bondorf, Proceedings of the European Conference on Nuclear Physics with Heavy Ions, J. Phys. C5, 195 (1976).

35. M.C. Robel and W. Swiatecki, private communication, 1978.

36. L.G. Moretto, private communication, 1978.

37. P. Bonche, S. Koonin and J.W. Negele, Phys. Rev. C13 1226 (1976).

38. C.Y. Wong, J.A. Maruhn and T.A. Welton, Phys. Lett. 66B, 19 (1977).

39. H.W. Bertini, R.T. Santoro and O.W. Hermann, Phys. Rev. C14, 590 (1976).

40. R.K. Smith and M. Janos, Proceedings of the Topical Conference on Heavy-Ion Collisions (Falls Creek, Tennessee, 1977), ORNL Publication CONF-770602, p. 363.

41. M. Gyulassy, Proceedings of the International Symposium on Nuclear Collisions and their Microscopic Descriptions, (Bled, Yugoslavia, 1977), Fizika 9(Supplement 4), 623 (1977).

FIGURE CAPTIONS

Fig. 1 Schematic Illustration of the Nuclear Fireball, which produces high temperature nuclear matter traveling with rapidity intermediate between projectile and target.

Fig. 2 The temperature of hot hadronic matter, assumed to be produced in a symmetric nuclear collision, is plotted as a function of the C. M. total energy per nucleon. The curve labelled "experimental" corresponds to a mass spectrum that approximates the known spectrum, while that labelled "Hagedorn" corresponds to the bootstrap model.

Fig. 3 Production cross sections of isotopes from the collisions of $^{16}O + ^{208}Pb$ at 137 MeV incident energy, plotted versus the two body ground state Q-value, Qgg. The slopes correspond to a dinuclear temperature ≈ 2 MeV.

Fig. 4 Momentum distribution of ^{10}Be fragments from the collision of 2.1 GeV/nucleon oxygen ions with carbon, plotted in the projectile rest frame. The gaussian peak is shifted slightly to negative p_{11} as required by the separation energy of the projectile into the fragments. The width of the distribution reflects the Fermi momentum, or the temperature.

Fig. 5 The variation of the temperature of the emitting system produced in the collision of $^{16}O + ^{208}Pb$, ^{197}Au as a function of the incident energy/nucleon (top scale), and the quantity $\sqrt{E_{CM}-V}$ (bottom scale). The open circles refer to temperatures deduced from isotope production cross sections and the closed circles from the momentum distributions.

Fig. 6 Energy spectra in the laboratory frame for ^{12}C fragments produced in the collision of ^{16}O + ^{208}Pb, ^{197}Au at different energies. The arrows E_p denote the energy of the fragment traveling with beam velocity, and E_F, E_F' the energies for fragmentation into ^{12}C together with an alpha particle or nucleons. The label g.s. denotes the energy for a two body reaction with both residual nuclei in the ground state.

Fig. 7 The variation with temperature of the lifetime for nucleon emission from the compound nucleus (t_p) and the relaxation time for dissipating the initial excitation over the nucleus (t_R).

Fig. 8 The in-plane angular correlation of alpha particles relative to ^{12}C (closed circles) and ^{16}O (open circles) in the collision of ^{16}O + ^{58}Ni at 6 MeV/nucleon.

Fig. 9 *In-plane correlations for* ^{16}O*-induced reactions on* ^{197}Au at 310 MeV (parts a-c) and on ^{208}Pb at 310 MeV (part d) and at 140 MeV (part e). Three different regions of Q-value are displayed Group I (part a,d,e): $Q(C-\alpha) \geq -20$ MeV, $Q(N-\alpha) \geq -30$ MeV. Group II (part b): -60 MeV $\leq Q(C-\alpha) < -20$ MeV, -80 MeV $\leq Q(N-\alpha) < -30$ MeV. Group III (part c): -100 MeV $\leq Q(C-\alpha) < -60$ MeV. Q is the three body Q-value. Only the $^{12}C-\alpha$ correlations corresponding to Group 1 exhibit two maxima as expected from kinematics of a quasi-free projectile break-up reaction.

Fig. 10 Schematic illustration of angular correlations between fast alpha particles and heavy fragments in quasi-elastic (QE) and deeply-inelastic (DI) collisions. In (a) the alpha particle production by radial friction leads to alpha particles and heavy fragments from deeply-inelastic scattering preferentially on the same side of the nucleus and on opposite sides for quasi-elastic scattering. The inverse correlations are illustrated in (b) where the alpha particles are assumed to be produced at the initial stage of the collision (sparking).

Fig. 11 Proton spectra produced in the bombardment of ^{58}Ni with ^{16}O ions at 10 MeV/nucleon and 20 MeV/nucleon. The cascade calculations shown superimposed on the 20 MeV/nucleon data were made for a similar system ^{12}C + Fe at 16 MeV/nucleon. The calculations reproduce the magnitude and slope of the data, and account for the production of such high energy protons (compared to the beam velocity) by decay in flight of the fast projectile.

Fig. 12 Two mechanisms of prompt nuclear emission in heavy-ion collisions. a) direct escape, b) escape after nucleon-nucleon collision.

Fig. 13 The density profiles obtained from a hydrodynamical calculation and a TDHF calculation for a collision energy of (E/A) = 100 MeV/nucleon. The numbers at the right of the figures give the time which is expressed in units of fm/c in the hydrodynamical calculations and in units of 10^{-21} sec. on the TDHF calculations. In both calculations matter is ejected with higher than beam velocity.

Fig. 14 Comparison of fireball model and cascade calculations for the $Ne + U \rightarrow p + x$ reaction.

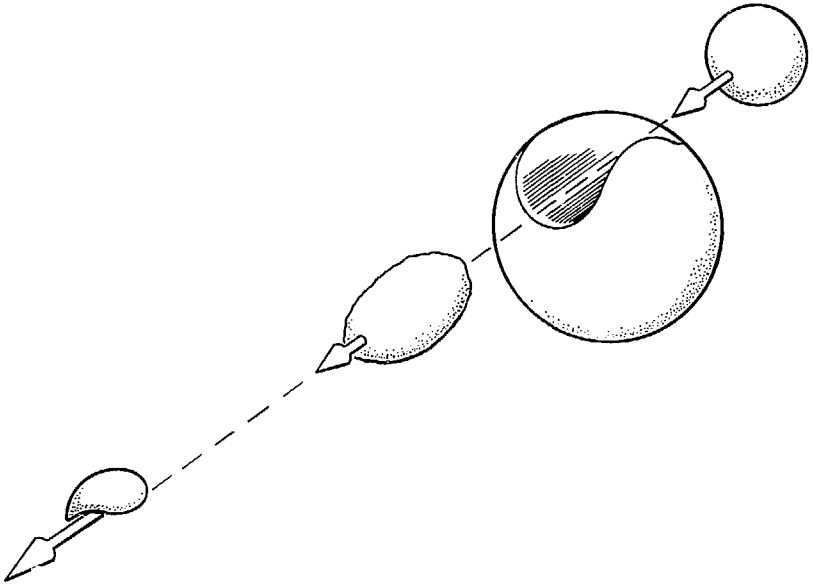

XBL 7610-4265

Fig. 1

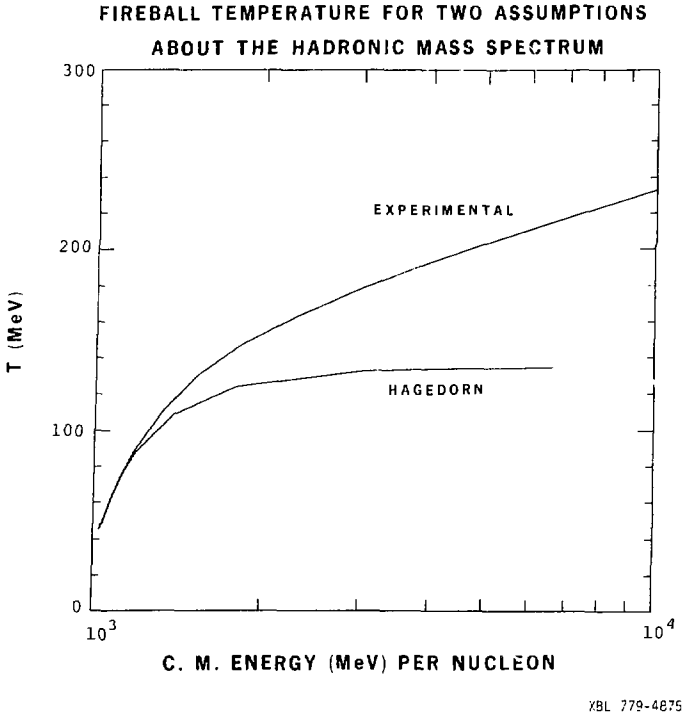

XBL 779-4875

Fig. 2

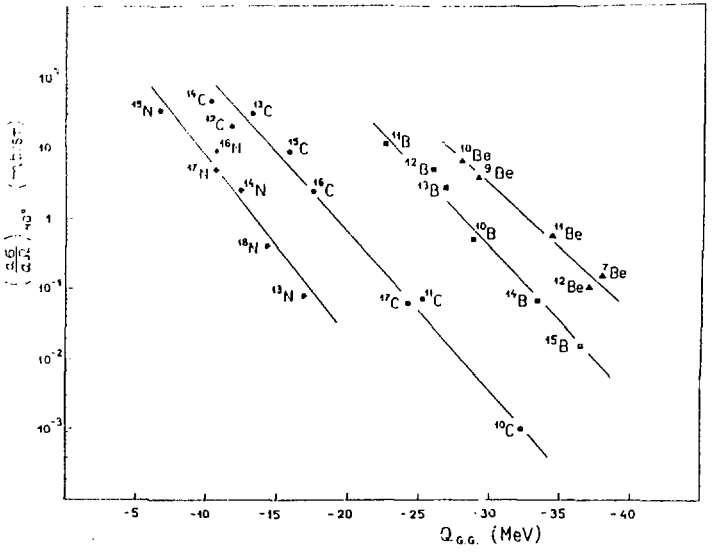

XBL 7779-38

Fig. 3

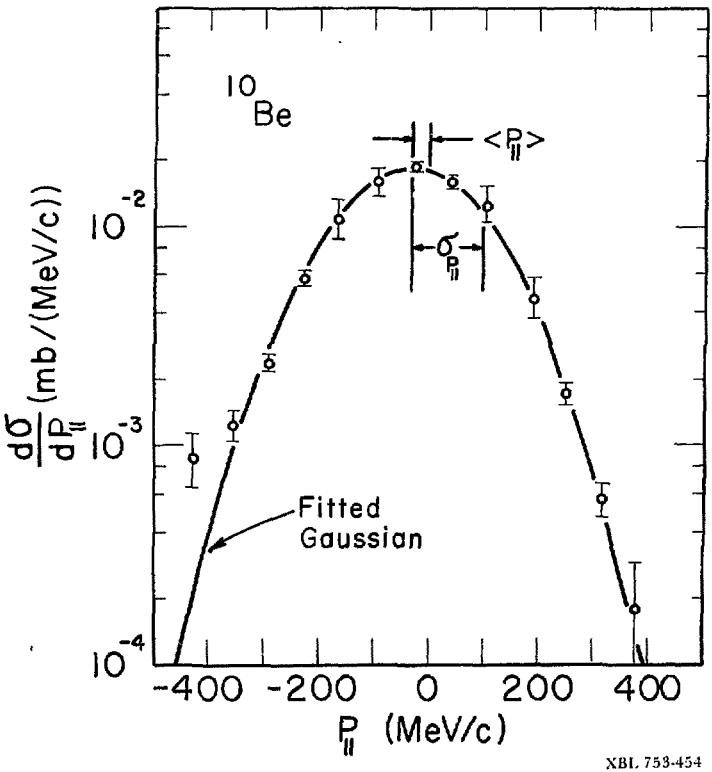
10 Be
<P∥>
σP∥
Fitted Gaussian
dσ/dP∥ (mb/(MeV/c))
10^-2
10^-3
10^-4
-400
-200
0
200
400
P∥ (MeV/c)
XBL 753-454

Fig. 4

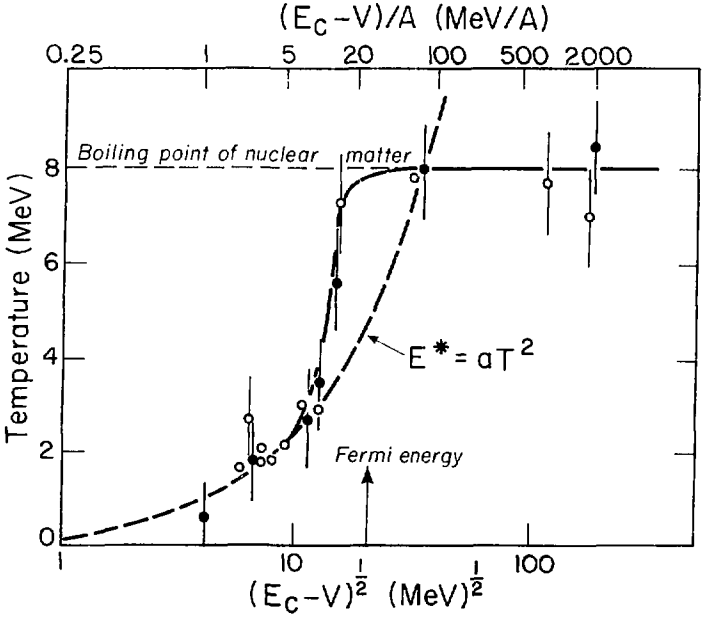
(E_C-V)/A (MeV/A)
0.25
1
5
20
100
500
2000
Boiling point of nuclear matter
Temperature (MeV)
8
6
4
2
0
E* = aT²
Fermi energy
1
10
100
(E_C-V)^½ (MeV)^½
XBL 783-503

Fig. 5

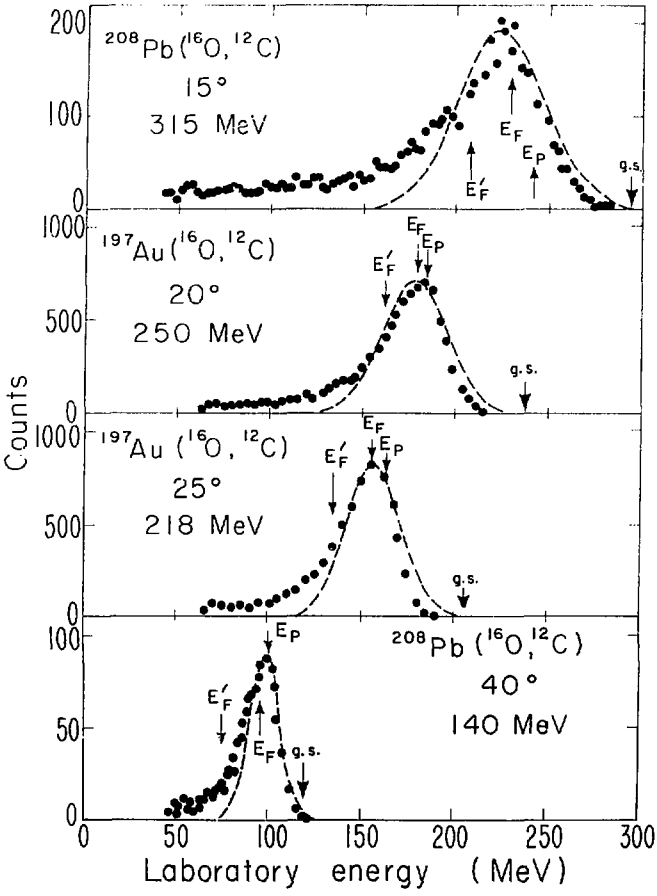

XBL7711-11041

Fig. 6

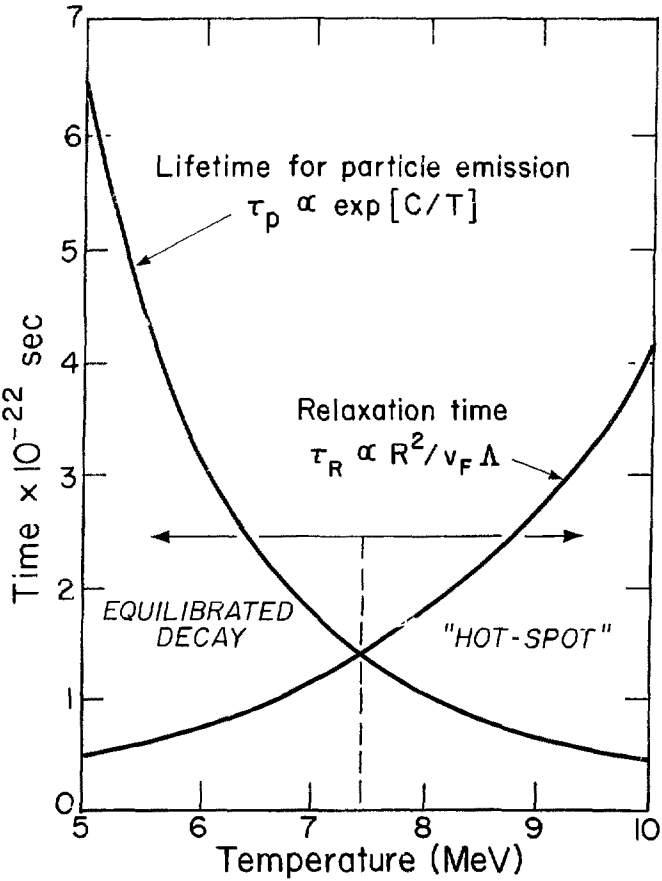

XBL 783-505

Fig. 7

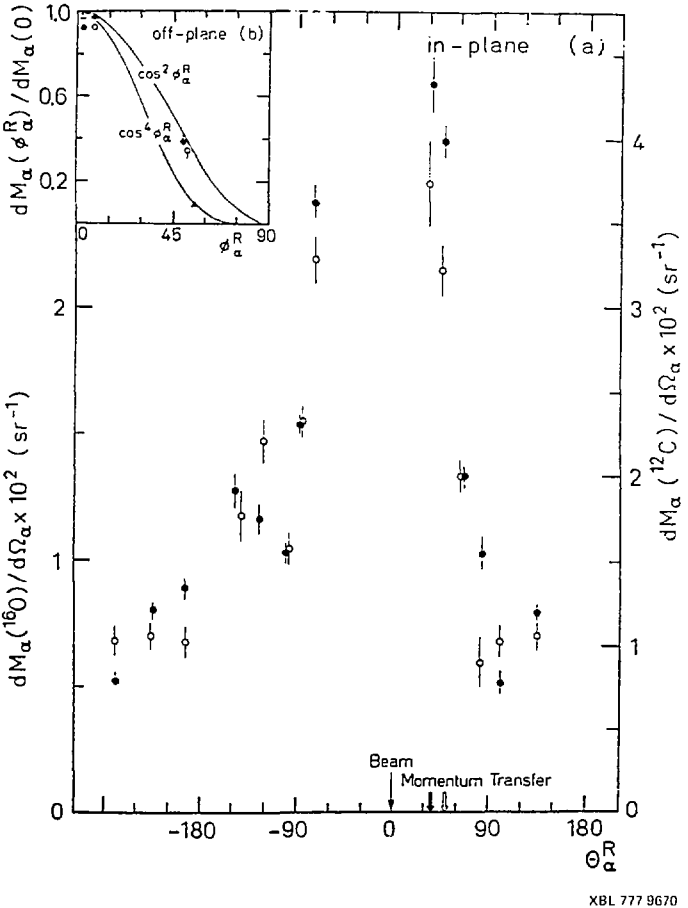
off-plane (b)
in-plane (a)
$\cos^2\phi_\alpha^R$
$\cos^4\phi_\alpha^R$
$dM_\alpha(\phi_\alpha^R)/dM_\alpha(0)$
ϕ_α^R
0
45
90
1.0
0.6
0.2
$dM_\alpha(^{16}O)/d\Omega_\alpha \times 10^2$ (sr^{-1})
$dM_\alpha(^{12}C)/d\Omega_\alpha \times 10^2$ (sr^{-1})
Beam
Momentum Transfer
-180
-90
0
90
180
Θ_α^R
XBL 777 9670

Fig. 8

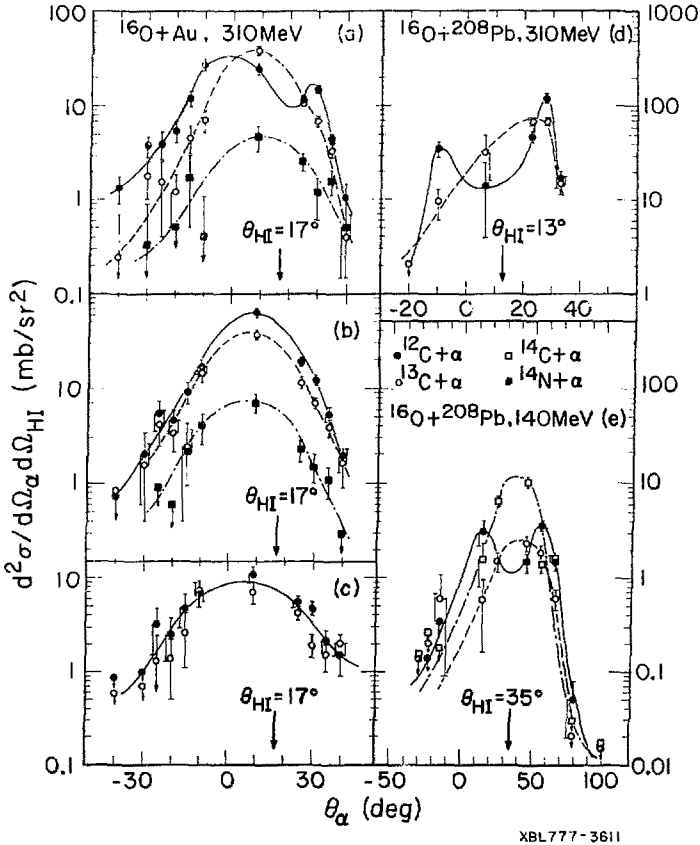
^{16}O+Au, 310MeV (a)
^{16}O+^{208}Pb, 310MeV (d)
(b)
(c)
^{16}O+^{208}Pb, 140MeV (e)
^{12}C+α
^{13}C+α
^{14}C+α
^{14}N+α
θ_{HI}=17°
θ_{HI}=13°
θ_{HI}=35°
$d^2\sigma/d\Omega_\alpha d\Omega_{HI}$ (mb/sr^2)
θ_α (deg)
XBL777-3611

Fig. 9

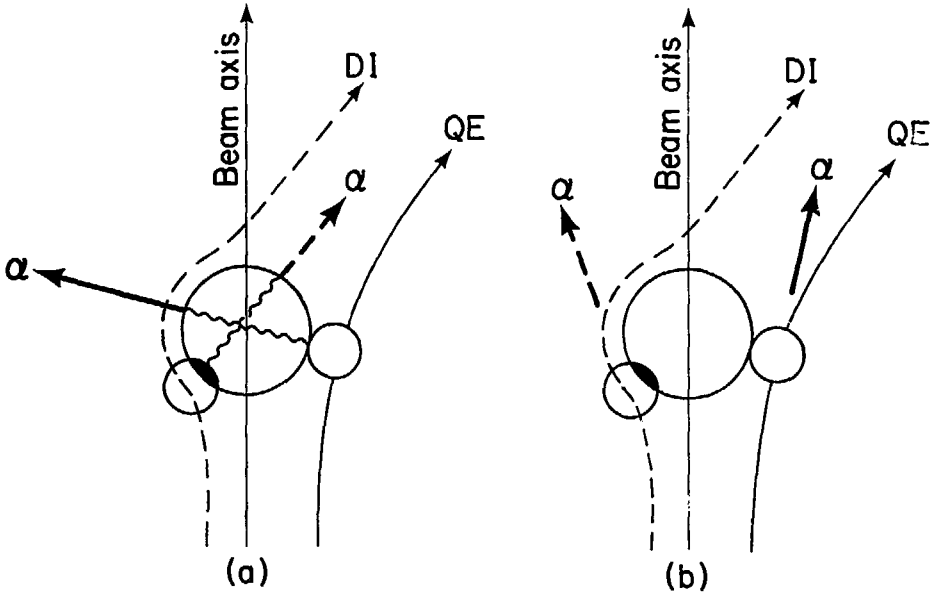

XBL 774-695

Fig. 10

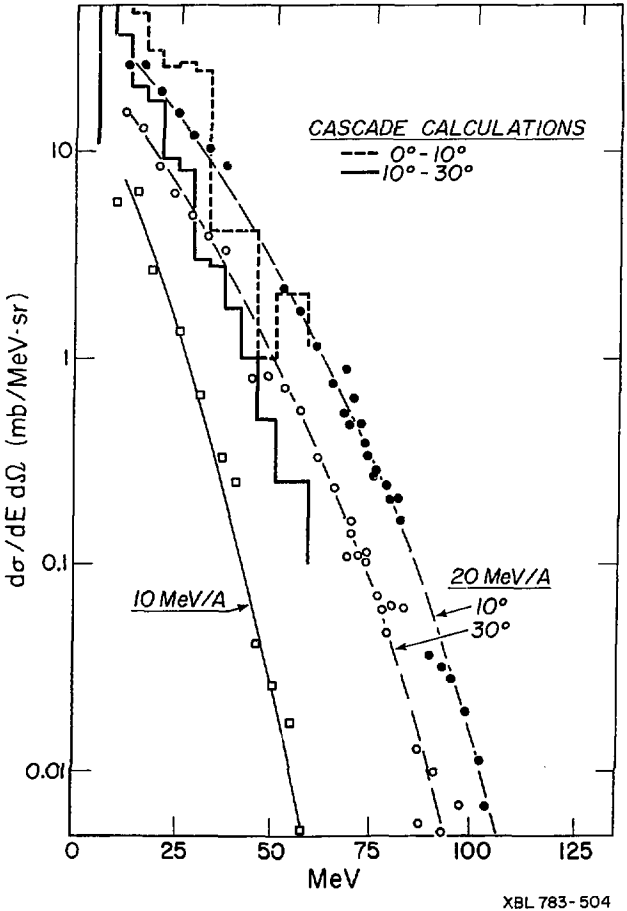
CASCADE CALCULATIONS
0°-10°
10°-30°
10
1
0.1
0.01
dσ/dE dΩ (mb/MeV-sr)
10 MeV/A
20 MeV/A
10°
30°
0
25
50
75
100
125
MeV
XBL 783-504

Fig. 11

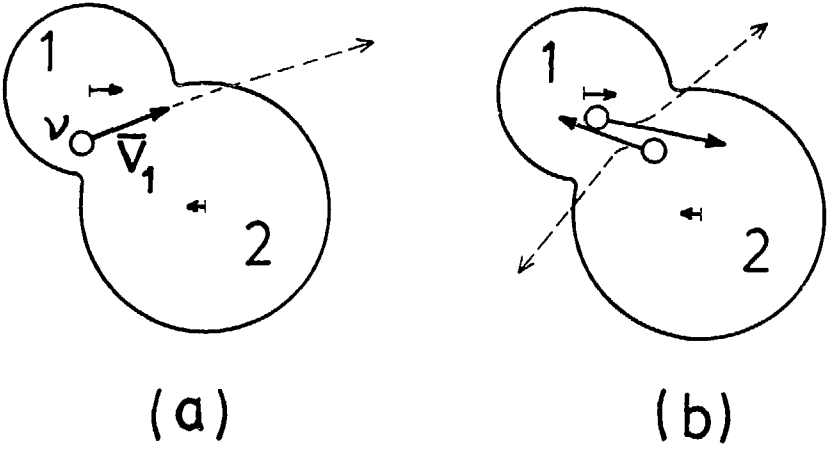

XBL 783-7746

Fig. 12

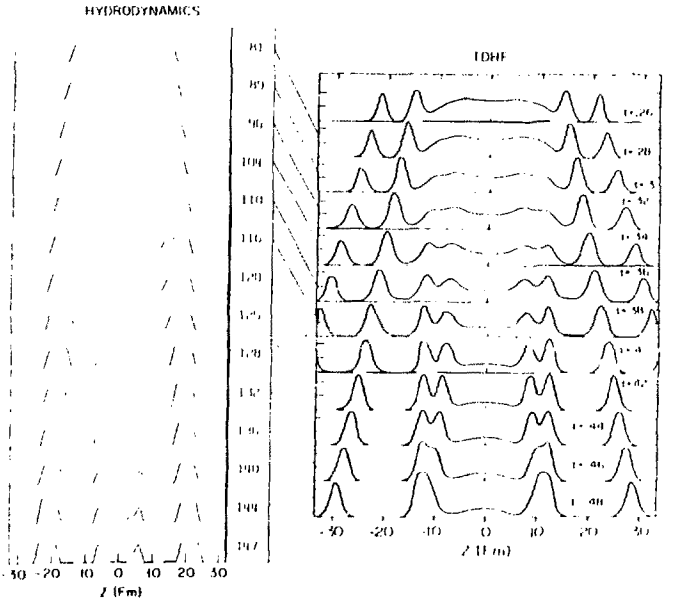

XBL 783-7747

Fig. 13

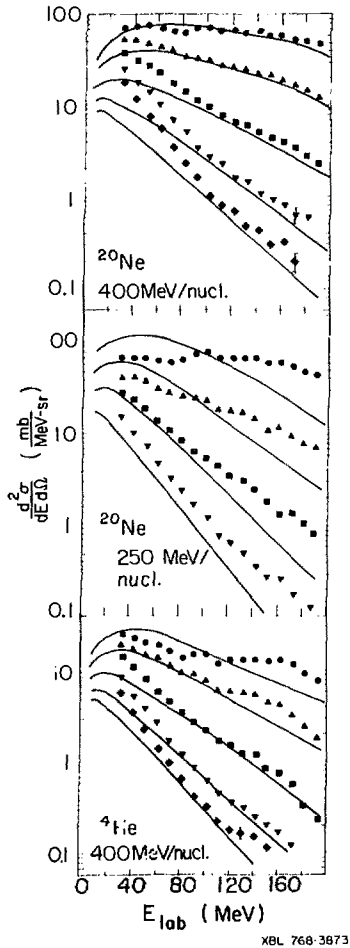

XBL 768-3873

Fig. 14a

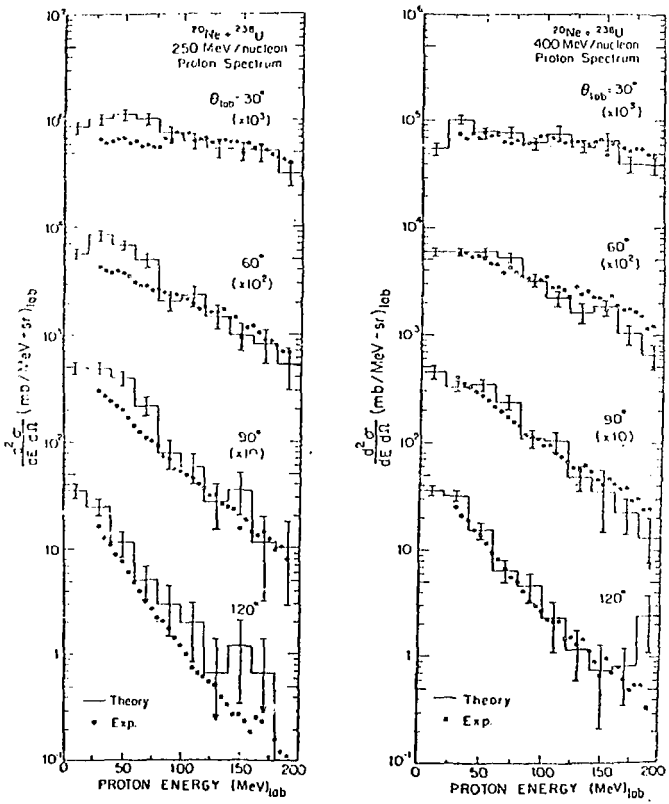

XBL 776-9233

Fig. 14b